Adsorption of Methane, Ethane, and Their Binary Mixtures on MCM-41: Experimental Evaluation of Methods for the Prediction of Adsorption Equilibrium

ARTICLE *in* LANGMUIR · FEBRUARY 2002

Impact Factor: 4.46 · DOI: 10.1021/la0155855

4 AUTHORS, INCLUDING:

Tina Düren
University of Bath
61 PUBLICATIONS **2,697** CITATIONS
SEE PROFILE

Frerich J Keil
Technische Universität Hamburg-Harburg
204 PUBLICATIONS **4,860** CITATIONS
SEE PROFILE

FK3608

Adsorption of Methane, Ethane, and Their Binary Mixtures on MCM-41: Experimental Evaluation of Methods for the Prediction of Adsorption Equilibrium

Jeong-Ho Yun,† Tina Düren,‡ Frerich J. Keil,‡ and Nigel A. Seaton*,†

School of Chemical Engineering, University of Edinburgh, King's Buildings, Edinburgh EH9 3JL, United Kingdom, and Verfahrenstechnik 4, Chemische Reaktionstechnik, Technische Universität Hamburg-Harburg, Eissendorfer Str. 38, D-21073 Hamburg, Germany

Received September 20, 2001. In Final Form: January 3, 2002

We report experimental measurements of the adsorption of methane and ethane, and binary mixtures of these components, on MCM-41. This adsorbent, which has a simple, regular pore structure and a chemically homogeneous surface, was used as a model system on which to evaluate methods for the prediction of adsorption equilibrium. Two methods were evaluated: ideal adsorbed solution theory and grand canonical Monte Carlo simulation. Both methods gave accurate predictions of binary adsorption. In addition, the grand canonical Monte Carlo method was able to accurately predict pure-component adsorption.

1. Introduction

MCM-41 materials have attracted considerable attention because of their remarkable features. They consist of hexagonally ordered arrays of long, unconnected cylindrical pore channels with diameters that can be varied within the range 15–100 Å, primarily by changing the alkyl chain length of the templating surfactants used in the synthesis procedure.[1,2] These well-defined structural characteristics suggest MCM-41 as a model adsorbent that could be used to test our understanding of adsorption at the molecular level and to evaluate methods for the prediction of adsorption equilibrium. MCM-41 materials have been extensively characterized, in terms of pore geometry, pore size distribution (PSD),[2–6] and pore wall thickness using X-ray diffraction (XRD),[1–4,7,8] transmission electron microscopy,[1,2,4] nuclear magnetic resonance,[2] and nitrogen adsorption.[1–4,7–10] The hydrothermal stability[11–15] and the reversibility of adsorption isotherms have also been studied.[16–18] The surface energy distribution of MCM-41 has also been investigated and found to be largely independent of both the pore size and the framework-substituted heteroatoms.[3,19]

The potential usefulness of MCM-41 mesoporous materials in industrial applications reflects their structural properties: large and controllable pore size with a narrow PSD and exceptionally high sorption capacities. Several studies have been performed of the adsorption on MCM-41 of aromatics,[2,20–23] alcohols,[20,24] ethylene,[16] *n*-hexane,[22] carbon dioxide,[16,17,25] carbon tetrachloride,[22,26,27] and methane.[25,28] In contrast to these studies of pure-gas adsorption, only one limited study of mixture adsorption has been reported.[25] Some Monte Carlo simulation results have been reported.[25,29–31]

Application areas of MCM-41, as a novel adsorbent or catalyst, have been suggested in gas storage systems,[28] VOC removal,[22,23] and liquid-phase adsorption.[32,33] Meanwhile, a presumed disadvantage was pointed out, namely that the low adsorption capacity at low partial pressures, which is due to the relatively large pore size (reflected in the typical type IV isotherm), might make MCM-41

* To whom correspondence should be addressed.
† University of Edinburgh.
‡ Technische Universität Hamburg-Harburg.

(1) Kresge, C. T.; Leonowicz, M. E.; Roth, W. J.; Vartuli, J. C.; Beck, J. S. *Nature* **1992**, *359*, 710.
(2) Beck, J. S.; Vartuli, J. C.; Roth, W. J.; Leonowicz, M. E.; Kresge, C. T.; Schmitt, K. D.; Chu, C. T-W.; Olsen, D. H.; Sheppard, E. W.; McCullen, S. B.; Higgins, J. B.; Schlenker, J. L. *J. Am. Chem. Soc.* **1992**, *114*, 10834.
(3) Kruk, M.; Jaroniec, M.; Sayari, A. *J. Phys. Chem. B* **1997**, *101*, 583.
(4) Kruk, M.; Jaroniec, M.; Sakamoto, Y.; Terasaki, O.; Ryoo, R.; Ko, C. H. *J. Phys. Chem. B* **2000**, *104*, 292.
(5) Sonwane, C. G.; Bhatia, S. K. *J. Phys. Chem. B* **2000**, *104*, 9099.
(6) Kruk, M.; Jaroniec, M. *Chem. Mater.* **2000**, *12*, 222.
(7) Sayari, A.; Liu, P.; Kruk, M.; Jaroniec, M. *Chem. Mater.* **1997**, *9*, 2499.
(8) Kruk, M.; Jaroniec, M.; Kim, J. M.; Ryoo, R. *Langmuir* **1999**, *15*, 5279.
(9) Kruk, M.; Jaroniec, M.; Sayari, A. *Langmuir* **1997**, *13*, 6267.
(10) Lukens, W. W.; Schmidt-Winkel, P.; Zhao, D.; Feng, J.; Stucky, G. D. *Langmuir* **1999**, *15*, 5403.
(11) Ryoo, R.; Kim, J. M. *J. Chem. Soc., Chem. Commun.* **1995**, 711.
(12) Ryoo, R.; Jun, S. *J. Phys. Chem. B* **1997**, *101*, 317.
(13) Ribeiro Carrott, M. M. L.; Estêvão Candeias, A. J.; Carrott, P. J. M.; Unger, K. K. *Langmuir* **1999**, *15*, 8895.
(14) Ribeiro Carrott, M. M. L.; Estêvão Candeias, A. J.; Carrott, P. J. M.; Sing, K. S. W.; Unger, K. K. *Langmuir* **2000**, *16*, 9103.
(15) Mokaya, R. *J. Phys. Chem. B* **2000**, *104*, 8279.
(16) Morishige, K.; Fujii, H.; Uga, M.; Kinukawa, D. *Langmuir* **1997**, *13*, 3494.
(17) Sonwane, C. G.; Bhatia, S. K.; Calos, N. *Ind. Eng. Chem. Res.* **1998**, *37*, 2271.
(18) Sonwane, C. G.; Bhatia, S. K. *Langmuir* **1999**, *15*, 5347.
(19) Kruk, M.; Jaroniec, M.; Sayari, A. *Langmuir* **1999**, *15*, 5683.
(20) Nguyen, C.; Sonwane, C. G.; Bhatia, S. K.; Do, D. D. *Langmuir* **1998**, *14*, 4950.
(21) Choudhary, V. R.; Mantari, K. *Langmuir* **2000**, *16*, 7031.
(22) Zhao, X. S.; Ma, Q.; Lu, G. Q. *Energy Fuels* **1998**, *12*, 1051.
(23) Hu, X.; Qaio, S.; Zhao, X. S.; Lu, G. Q. *Ind. Eng. Chem. Res.* **2001**, *40*, 862.
(24) Branton, P. J.; Hall, P. G.; Sing, K. S. W. *Adsorption* **1995**, *1*, 77.
(25) Koh, C. A.; Montanari, R. I.; Nooney, S. F.; Tahir, S. F.; Westacott, R. E. *Langmuir* **1999**, *15*, 6043.
(26) Branton, P. J.; Sing, K. S. W.; White, J. W. *J. Chem. Soc., Faraday Trans.* **1997**, *93*, 2337.
(27) Branton, P. J.; Reynolds, P. A.; Studer, A.; Sing, K. S. W.; White, J. W. *Adsorption* **1999**, *5*, 91.
(28) Ioneva, M. A.; Newman, G. K.; Harwell, J. H. *AIChE Symp. Ser.* **1995**, *91* (309), 40.
(29) Maddox, M. W.; Gubbins, K. E. *Int. J. Thermophys.* **1994**, *15*, 1115.
(30) Maddox, M. W.; Sowers, S. L.; Gubbins, K. E. *Adsorption* **1996**, *2*, 23.
(31) Maddox, M. W.; Olivier, J. P.; Gubbins, K. E. *Langmuir* **1997**, *13*, 1737.
(32) Meziani, M. J.; Zajac, J.; Partyka, S. *Langmuir* **2000**, *16*, 8410.
(33) Piwonski, I.; Zajac, J.; Jones, D. J.; Rozière, J.; Partyka, S.; Plaza, S. *Langmuir* **2000**, *16*, 9488.

10.1021/la0155855 CCC: $22.00
Published on Web 02/08/2002

unsuitable for purification processes.[22,23] However, a technique to control the pore size using chemical vapor deposition has been suggested to overcome this weakness.[34]

The main aim of this study is to investigate the fundamental basis of classical and statistical mechanical methods for the prediction of adsorption equilibrium. Because of its regular structure, MCM-41 is the adsorbent used, but the intention is to make a broader judgment about these methods, by viewing MCM-41 as a highly ordered and well-characterized prototype of a nonpolar (in the pure silica form used in this study) adsorbent. The adsorptive gases studied are methane, ethane (both nonpolar gases), and mixtures of these components. The predictive methods we have studied are (i) ideal adsorbed solution theory (IAST),[35] an engineering thermodynamic model, and (ii) grand canonical Monte Carlo (GCMC) simulation, a statistical mechanical method, to predict adsorption in MCM-41.

2. Experimental Section

Materials. Pure silica MCM-41 materials were supplied by Chonnam National University, Korea. The samples had been prepared using hexadecyltrimethylammonium bromide (HTABr, $C_{16}H_{33}(CH_3)_3NBr$, Aldrich) as a surfactant template and Ludox HS40 (Du Pont) as a source of silica. The synthesis procedures are described in refs 1, 2, and 36–38. MCM-41 mesoporous materials are highly dispersed amorphous powders. In a bench-scale adsorption experiment, such a powdery sample needs to be compacted with a high pressure into pellets because powdery samples will otherwise cause an undesirable pressure drop in the adsorber. Concerning the mechanical stability of MCM-41 after compacting with high pressures, Gusev et al.[39] have reported a valuable case study using nitrogen adsorption and XRD analysis. According to their results, the ordered structure of pure silica MCM-41 can drastically be altered by external pressures and eventually destroyed at a very high pressure of 224 MPa. To minimize structural alteration, our samples were compressed by using a hand-operated press (Spectroscopy Central) with a relatively small external pressure of 2 MPa for about 3 s. Then the compressed MCM-41 samples were crushed to 10–12 mesh and calcined at 500 °C for 12 h, 200 °C for 4 h, and 120 °C for 2 h, in sequence, prior to use.

The XRD pattern (Siemens D5000) and nitrogen isotherm at 77 K (Micromeritics ASAP 2010) were examined for both before and after preparation (i.e. compression, calcination, and crushing), to see if there was any significant alteration in their properties. It can be seen from XRD diffraction patterns (Figure 1) that the four peaks, which are typical for MCM-41 materials,[1,2] are observed for both samples with almost the same intensity and position, which indicates the original properties were retained after preparation. The interplanar spacing d_{100} values are very similar for both samples: 39.4 Å (original material) and 38.8 Å (after preparation). The evidence for the retention of the structural properties is also provided by the results of nitrogen isotherms at 77 K, as shown in Figure 2. The isotherms for both samples are nearly identical with a steep, reversible pore-filling step over a narrow range of the relative pressure, which indicates high pore size uniformity. The BET specific surface areas and BJH (Barrett, E. P.; Joyner, L. G.; Halenda, P. H. *J. Am. Chem. Soc.* **1951**, *73*, 373) average pore diameters are found to be very similar for both samples: 1042 m^2/g and 40.6 Å (original material) and 1023 m^2/g and 40.9 Å (after preparation). In summary, the preparation of the samples for the adsorption experiment had little effect on the structure of the adsorbent.

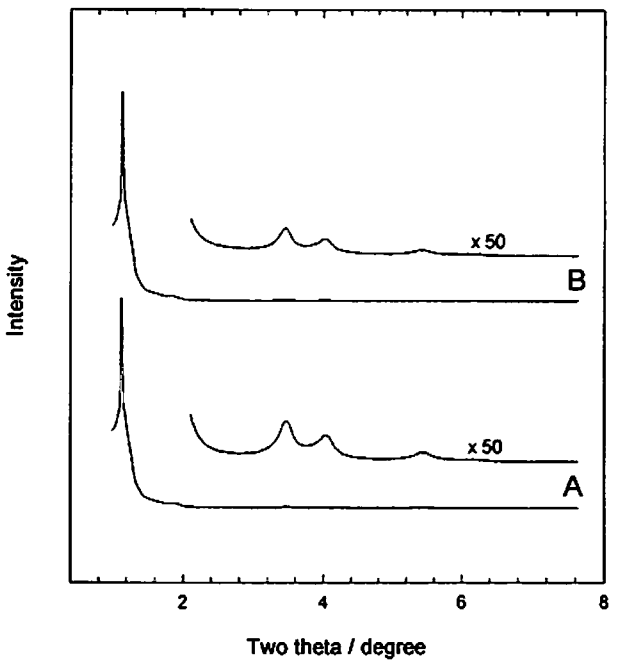

Figure 1. Powder X-ray diffraction patterns for the MCM-41 samples: (A) original MCM-41 material; (B) MCM-41 material after compression, calcination, and grinding.

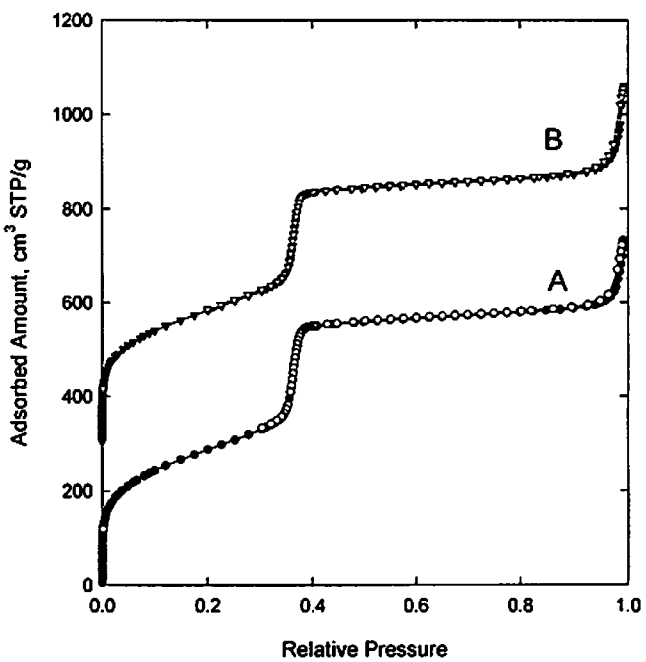

Figure 2. Nitrogen adsorption isotherms for the MCM-41 samples: (A) original MCM-41 material; (B) MCM-41 material after compression, calcination, and grinding (adsorption, filled symbols; desorption, open symbols). The isotherm for sample B is shifted upward by 300 cm^3 STP/g.

The adsorptive gases, methane and ethane, were purchased from BOC Co., and the purity of these gases was 99.99%. Beds packed with 5A molecular sieve were used to dry the gases from cylinders.

Apparatus and Procedure. The adsorption equilibria for pure methane and ethane and their binary mixtures on the MCM-41 were determined using a bench-scale open-flow adsorption/desorption apparatus.[40,41] A schematic diagram of the apparatus

(34) Zhao, X. S.; Lu, G. Q.; Hu, X. *J. Chem. Soc., Chem. Commun.* **1999**, 1391.
(35) Myers, A. L.; Prausnitz, J. M. *AIChE J.* **1965**, *11*, 121.
(36) Kresge, C. T.; Leonowicz, M. E.; Roth, W. J.; Vartuli, J. C. US. Patent 5098 643, 1992.
(37) Kresge, C. T.; Leonowicz, M. E.; Roth, W. J.; Vartuli, J. C. US. Patent 5098 684, 1992.
(38) Seo, G.; Kim, N.-H.; Lee, Y.-H.; Kim, J.-H. *Catal. Lett.* **1999**, *57*, 209.
(39) Gusev, V. Y.; Feng, X.; Bu, Z.; Haller, G. L.; O'Brien, J. A. *J. Phys. Chem.* **1996**, *100*, 1985.
(40) Talu, O.; Zwiebel, I. *AIChE J.* **1986**, *32*, 1263.

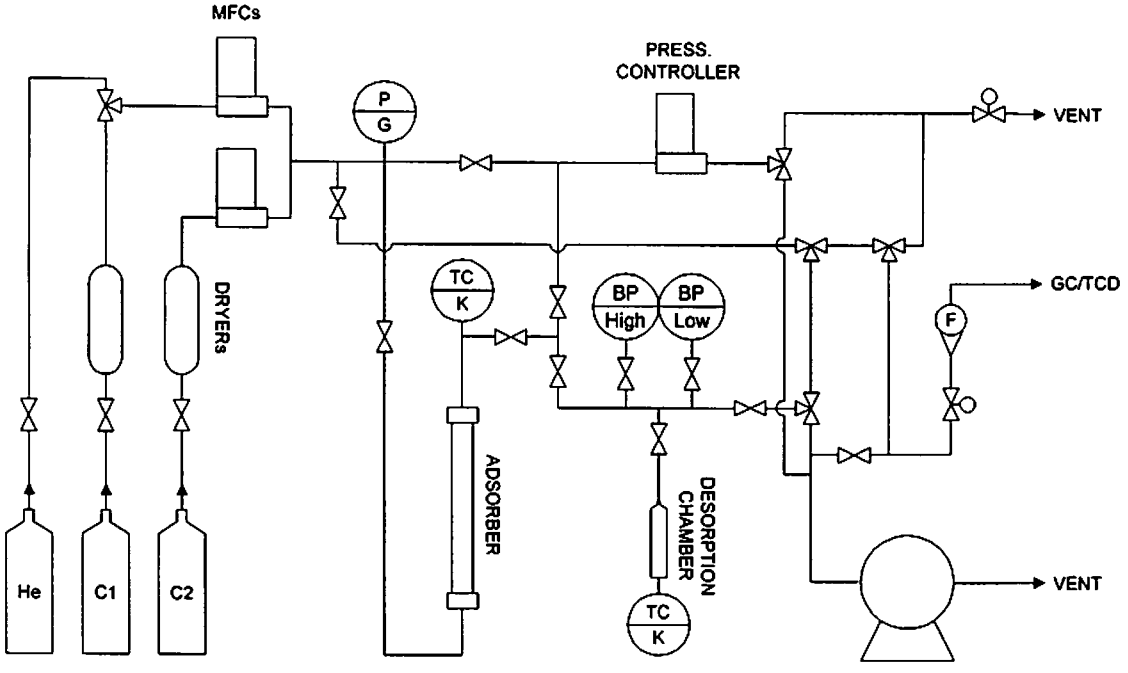

Figure 3. Schematic diagram of the adsorption apparatus used in this study.

is shown in Figure 3. The apparatus allows both the static volumetric measurement of pure-component isotherms and the measurement of mixture adsorption using a flow-through measurement technique, at pressures up to 33 bar and at temperatures from 263 to 274 K. In this study, a 6.75 g sample of dried, compressed MCM-41 was used in all the experiments. The system pressure measurements were performed with two Baratron absolute pressure transducers (MKS type 127A) with a two-channel readout/signal conditioner (MKS type PR4000). Their pressure ranges are from 0 to 133.33 kPa and from 0 to 3333.25 kPa, respectively, and the reading accuracy is 0.05% of the usable measurement range. During all experiments, the adsorber was placed in a water bath and temperature was maintained within ±0.02 K with a refrigerating/heating circulator (Julabo type F25).

Preceding each pure-component isotherm measurement, regeneration of the MCM-41 sample was carried out at 523 K under a vacuum of less than 2×10^{-3} Torr generated with a rotary pump (Edward type RV5) for at least 2 h. The degree of vacuum was monitored with a vacuum gauge (Edward type Active Pirani Gauge). Prior to the experiment, the volumes of the charged adsorber and the desorption chamber were determined by the expansion of helium gas. The operating procedure for pure-component isotherm determination is to admit gas into the desorption chamber, to measure its temperature and pressure, to expand the gas into the adsorber, and finally to record the equilibrium temperature and pressure. The knowledge of pressure, temperature, and gas volume before and after each step gives the number of moles of gas before and after the adsorption and, by difference, the moles adsorbed. In this study, the Peng–Robinson equation of state was employed for the calculation of the number of moles in the gas phase. The uncertainty of the pure species isotherm data obtained in this study is less than 0.2%.

In the flow-through desorption method, for binary isotherm measurement, a gas mixture flows through the adsorber, at a desired condition of system pressure, temperature, and gas composition. Two mass flow controllers (Brooks type 5850), a back-pressure controller (Brooks type 5866), and a read out/control device (Brooks type 0154) are used to obtain a constant gas composition and a constant system pressure. The composition of the gas leaving the adsorber is measured with a gas chromatograph (Shimadzu GC-14B, equipped with a thermal conductivity detector). The gas mixture continues to flow through the adsorber until adsorption equilibrium is attained, which is defined to be when the inlet and outlet gas streams of the adsorber have equal compositions (to within experimental error) for at least 1 h. Then, both the adsorbed material and gas-phase contents of the adsorber are transferred to the previously evacuated desorption chamber (of known volume) by heating the adsorber at 523 K and cooling the desorption chamber with liquid nitrogen. After desorption is complete and the desorption chamber temperature has returned to ambient temperature overnight, the desorption chamber pressure is recorded and the composition of the mixture in the chamber is analyzed with the gas chromatograph. The number of moles of each component adsorbed is determined by subtracting the number of moles in the void space of the adsorber (calculated from the pressure, the temperature, the measured volume, and the known composition of the gas phase, using the Peng–Robinson equation) from the number of moles of that component in the desorption chamber. The uncertainty of the binary isotherm data obtained in this study is less than 1.5%.

3. Ideal Adsorbed Solution Theory

Ideal adsorbed solution theory (IAST)[35] is a widely used engineering thermodynamic method, analogous to Raoult's law in vapor–liquid equilibrium. The inputs to the IAST calculation are the pure-component adsorption isotherms at the temperature of interest, and the output is a prediction of the mixture equilibrium. The structure of the adsorbent does not appear explicitly. Deviations from IAST might result from the chemical dissimilarity of the adsorptive species (as for deviations from Raoult's law in vapor–liquid equilibrium) or from the heterogeneity of the adsorbent. Adsorbent heterogeneity might be present in one of several forms: chemical or structural heterogeneity of the adsorbent surface,[42] variation of pore size and shape (either along the axis of individual pores or among the pores), or due to connectivity effects.[43,44] Indeed, recent simulations of the structure of noncrystalline adsorbents over length scales much larger than individual pores suggest structures that are highly disordered on a

(41) Heuchel, M.; Davies, G. M.; Buss, E.; Seaton, N. A. *Langmuir* **1999**, *15*, 8695.

(42) Rudzinski, W.; Everett, D. M. *Adsorption of Gases on Heterogeneous Surfaces*; Academic Press: New York, 1992.

(43) López-Ramón, M. V.; Jagiello, J.; Bandosz, T. J.; Seaton, N. A. *Langmuir* **1997**, *13*, 4435.

(44) Davies, G. M.; Seaton, N. A. *Langmuir* **1999**, *15*, 6263.

Table 1. Toth Parameters To Represent Pure Methane Isotherm Data at 264.75 K

$a = 1.193\,12 \times 10^{1}$
$b = 2.428\,00 \times 10^{2}$
$c = 6.598\,41 \times 10^{-1}$
avg error = 0.706%

range of length scales, where these forms of heterogeneity are interwoven.[45,46] Nonideal adsorption can be accommodated in the general framework of adsorbed solution theory by real adsorbed solution theory (RAST),[35] in which nonideal interactions between the components are accounted for by activity coefficients, and by heterogeneous ideal adsorbed solution theory (HIAST),[47] in which the energetic heterogeneity of the adsorbent is taken into account.

Many adsorbents are highly heterogeneous in one sense or another. This is almost always the case for industrial adsorbents, where the two main classes are zeolites, which are both chemically and physically heterogeneous at the scale of individual pores, and activated carbons, which have relatively homogeneous surfaces but are heterogeneous at the pore network level (having a distribution of pore sizes). Despite this, IAST often gives very accurate predictions; for example, mixtures of nonpolar components on carbon are often (though not always[48]) accurately predicted by IAST, suggesting that the adsorbent heterogeneity is insufficient in such cases to invalidate IAST. One can thus regard the utility of IAST as having been empirically proven.

Nevertheless, it is of fundamental interest to test IAST on a model adsorbent, which is homogeneous in all senses. MCM-41 has a simple pore shape, and its surface is chemically homogeneous (in the pure silica form used here). While the surface is atomically disordered (as MCM-41 is noncrystalline), compared with adsorbents used in practical adsorption applications (e.g. carbons or zeolites) this is a highly homogeneous adsorbent. Similarly, as the two adsorptives—methane and ethane —are chemically similar, one would not expect nonideal adsorbate–adsorbate interactions.

Subject to the assumption of an ideal adsorbed phase, equality of chemical potential in the bulk gas and adsorbed phases implies[35]

$$\bar{f}_i = x_i f_i^{\circ}(\pi) \tag{1}$$

where $\bar{f}_i$ is the fugacity of component i in the bulk gas phase and x_i is the mole fraction of component i in the adsorbed phase; f_i° is the standard-state fugacity, that is, the fugacity of pure component i at the mixture spreading pressure, π, when the adsorbed and bulk gas phases are in equilibrium. The spreading pressure is obtained from the experimental adsorption isotherm, $n_i(P)$, via the Gibbs adsorption isotherm:

$$\frac{\pi A}{RT} = \int_0^{f_i^{\circ}} n_i \, \mathrm{d} \ln f_i \tag{2}$$

where A is the surface area of the adsorbent (which is not required in practice, as the product πA need not be separated in the calculation), R is the gas constant, T is the temperature, and f_i is the fugacity of pure component i. The complete description of multicomponent adsorption equilibria requires an expression for total amount adsorbed, n_t:

$$\frac{1}{n_t} = \sum_i \frac{x_i}{n_i^{\circ}} \tag{3}$$

where n_i° is the amount of component i adsorbed at the standard-state pressure.

To calculate the spreading pressure using eq 2, the pure-component isotherms must first be fitted to a suitable isotherm equation to an acceptable degree of accuracy. Methane has an IUPAC type I isotherm, which was fitted by the Toth isotherm:[49]

$$n = \frac{aP}{(b + P^c)^{1/c}} \tag{4}$$

The fitted values of the parameters a, b, and c are given in Table 1. The near-critical isotherms of ethane are of IUPAC type IV, and this more complex shape is more difficult to represent by a simple analytical isotherm equation. Although some suggested isotherm models, which have been recommended for the type IV isotherm,[50] were considered, their accuracy was insufficient for the evaluation of pure-component spreading pressure. As pointed out by Yun et al.,[51] in IAST calculations, there is no restriction on the choice of pure-component isotherm. A piecewise fitting technique is an alternative approach to describing a complex equilibrium isotherm, and this approach was followed in this study. First, the whole ethane isotherm at 264.75 K was split up into five pressure ranges based on the shape of the isotherm, as illustrated in Figure 4. As seen in the figure, the ethane isotherm begins with a region of favorable adsorption, that is, one in which the isotherm has negative curvature (I), which is then followed by a linear region (II), an unfavorable region (III), and a favorable region (IV), and finally reaches an unfavorable region (V). In Table 2, the fitting equations used in each pressure range are presented along with the fitting parameters.

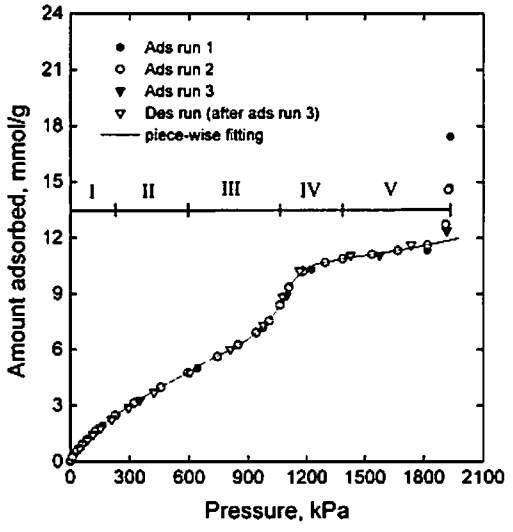

Figure 4. Representation of pure ethane isotherm data at 264.75 K by piecewise fitting.

(45) Thomson, K. T.; Gubbins, K. E. *Langmuir* **2000**, *16*, 5761.
(46) Sarkisov, L.; Monson, P. A. *Langmuir* **2000**, *16*, 9857.
(47) Valenzuela, D.; Myers, A. L.; Talu, O.; Zwiebel, I. *AIChE J.* **1988**, *34*, 397.
(48) Yang, R. T. *Gas Separation by Adsorption Processes*; Butterworth: Boston, 1987.
(49) Toth, J. *Acta Chim. Acad. Sci. Hung.* **1962**, *32*, 39.
(50) Martinez, G. M.; Basmadjian, D. *Chem. Eng. Sci.* **1996**, *51*, 1043.
(51) Yun, J.-H.; Park, H. C.; Moon, H. *Korean J. Chem. Eng.* **1996**, *13*, 246.

Table 2. Fitting Equations and Parameters to Represent Pure Ethane Isotherm Data at 264.75 K

	value for the following pressure ranges and fitting equations				
		P/kPa = 228.3−594.4[b]			P/kPa = 1384.4−max.[e]
param	P/kPa = 0.0−228.3[a] Toth isotherm	$n = aP/(b + P) + cP/(d + P)$	P/kPa = 594.4−1062.2[c]	P/kPa = 1062.2−1384.4[d] $n = a + bP + cP^2 + dP^3$	$n = (a + bP + cP^2)/(1 + dP + eP^2 + fP^3)$
a	$1.314\,53 \times 10^2$	$1.075\,40 \times 10^0$	$-1.270\,78 \times 10^1$	$-2.515\,35 \times 10^2$	$7.282\,73 \times 10^0$
b	$1.102\,24 \times 10^1$	$7.391\,13 \times 10^1$	$6.375\,73 \times 10^{-2}$	$5.944\,04 \times 10^{-1}$	$1.412\,47 \times 10^{-2}$
c	$2.948\,44 \times 10^{-1}$	$2.022\,74 \times 10^1$	$-7.867\,75 \times 10^{-5}$	$-4.503\,49 \times 10^{-4}$	$7.016\,35 \times 10^{-6}$
d		$2.550\,84 \times 10^3$	$3.517\,34 \times 10^{-8}$	$1.140\,69 \times 10^{-7}$	$-2.049\,71 \times 10^{-3}$
e					$1.224\,22 \times 10^{-6}$
f					$1.510\,36 \times 10^{-10}$

[a] Range no. I. [b] Range no. II. [c] Range no. III. [d] Range no. IV. [e] Range no. V.

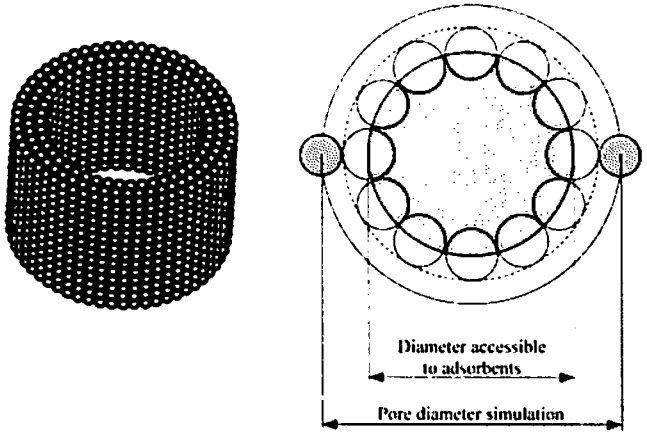

Figure 5. (a, left) Model pore. (b, right) Definition of pore diameter in experiment and simulation. The shaded area is used to calculate V_i^{bulk}.

4. Molecular Simulation

In contrast to IAST, grand canonical Monte Carlo (GCMC) simulation is a statistical−mechanical method, in which a rigorous molecular-level model of adsorption is solved exactly (in principle—i.e., the error can be reduced to an arbitrarily small value if a sufficiently large system is simulated for a sufficiently long time). In the grand canonical ensemble, the chemical potential of each component, the temperature, and the volume of the adsorbent are kept constant, as in real adsorption experiments, while the number of molecules of each component in the adsorbed phase fluctuates. The chemical potential is related to the bulk pressure and composition by an equation of state. As in the analysis of experimental data, and in IAST calculations, the Peng−Robinson equation was used in the simulations. The average properties of an adsorbate in a model pore of given volume are calculated by sampling configurations that are consistent with the temperature and the chemical potentials of the components present. Successive configurations are obtained by attempting to move, add, and remove molecules, and by accepting each new, "trial" configuration probabilistically, according to the appropriate Boltzmann factor. In the case of a binary mixture, identity swaps are additionally attempted. In each MC step, one of these actions is chosen with equal probability. A general description of the GCMC method can be found for example in refs 52 and 53.

Although MCM-41 has a honeycomb structure that results from the hexagonal packing of unidimensional cylindrical pores[54] and NMR studies suggest an amorphous structure for the pore walls closely related to amorphous silica,[17] a regular pore model was employed to keep the model as simple as possible. The MCM-41 model pore consists of a regular array of oxygen atoms arranged on a rectangular grid on three concentric cylinders (see Figure 5). Three wall layers give a wall thickness of about 10 Å—a value typical for MCM-41.[54] The silicon atoms in the adsorbent are ignored, as their effect on adsorption is very slight.[55] The density of the oxygen atoms in the model pore corresponds to the skeletal density of amorphous silica (2.2 g/cm).[54] To include the roughness of the pore wall in the model pore, the interaction of an adsorbate molecule with every atom in the pore wall is calculated rather than using an averaged potential.

Table 3. Lennard-Jones Parameters Used in GCMC Simulations

molecule	ϵ/k_B, K	σ, Å	bond length, Å
CH_4[56]	149.92	3.7327	
C_2H_6 (2CLJ)[56]	139.8	3.512	2.353
O	185[a]	2.708[25]	

[a] Optimized to reproduce the pure ethane adsorption isotherm at 264.75 K.

The fluid−fluid and the fluid−wall interactions were modeled with the truncated Lennard-Jones potential:

$$u_{ij}(r) = \begin{cases} 4\epsilon_{ij}\left[\left(\frac{\sigma_{ij}}{r}\right)^{12} - \left(\frac{\sigma_{ij}}{r}\right)^{6}\right] & r \le r_{cut} \\ 0 & r > r_{cut} \end{cases} \quad (5)$$

Here r is the distance between two interacting molecules of species i and j, and r_{cut} is the cutoff radius. All interactions were truncated at $3.5\sigma_{CH_4}$. The Lorentz−Berthelot mixing rules were used for calculating the mixed Lennard-Jones parameters. No long-range corrections were applied. Methane and ethane were represented by united-atom models. Methane was represented by a single Lennard-Jones interaction site whereas the linear ethane molecule was described by two Lennard-Jones sites. The Lennard-Jones parameters used in this work are summarized in Table 3.

The GCMC simulations were carried out in a simulation cell containing a section of the model pore, and periodic boundary conditions were applied along the axis of the pore. The simulation cell had a length of 40 Å, which was sufficiently large to make the effect of finite system size negligible. The initial configuration was generated by placing one molecule randomly in the model pore. The system was then equilibrated for 500 000 GCMC steps,

(52) Allen, M. P.; Tildesley, D. J. *Computer simulations of liquids*; Clarendon Press: Oxford, 1987.
(53) Frenkel, D.; Smit, B. *Understanding molecular simulations*; Academic Press: San Diego, 1996.
(54) Ciesla, U.; Schüth, F. *Microporous Mesoporous Mater.* **1999**, *27*, 131.
(55) Bezus, A. G.; Kiselev, A. V.; Lopatkin, A. A.; Pham Quang Du. *J. Chem. Soc., Faraday Trans. 2* **1978**, *74*, 367.

and data were collected for another 500 000 GCMC steps to get the average amount adsorbed. Complete isotherms were determined by successively varying either the pressure or the bulk-phase composition.

The output of such a simulation is the absolute density of the adsorbate, that is, the average number of molecules in the model pore. As the experimental data represent excess adsorption, the simulation results had to be converted to absolute isotherms. This was done as described in ref 41. The excess number of molecules of species i, $N_i^{ex}(d,T,P,y)$, is related to the absolute, that is, simulated number of molecules, N_i^{abs}, by

$$N_i^{ex}(d,T,P,y) = N_i^{abs}(T,P,y) - y_i\rho_i^{bulk}(T,P)\,V_i^{bulk}(d) \quad (6)$$

where d is the diameter of the model pore, $\rho_i^{bulk}(T,P)$ is the bulk fluid density at the specified temperature and pressure calculated with the Peng–Robinson equation, and V_i^{bulk} is the volume in the model pore that is accessible to component i, given by

$$V_i^{bulk} = \frac{\pi}{4}l(d - \sigma_i - \sigma_O) \quad (7)$$

where l is the pore length, d is the pore diameter measured from the centers of the atoms on the surface of the pore wall, and σ_i and σ_O are the Lennard-Jones parameters of species i and the oxygen of the pore wall (see Figure 5). The excess adsorbate density ρ_i is then obtained by dividing the excess number of particles adsorbed by the volume of the simulation cell:

$$\rho_i(d,T,P,y) = \frac{N_i^{ex}(d,T,P,y)}{\pi d^2 l} \quad (8)$$

To compare the GCMC simulation results, which yield the adsorbate density in millimoles per cubic centimeter, with the experimental density that is measured in millimoles per gram, the porosity is taken as a conversion factor. As the exact structure of our MCM-41 sample (i.e. the thickness of the pore walls) is not known, the number of oxygen atoms in our model pore cannot be used for the conversion. The porosity was therefore fixed by fitting the simulation results to experimental data for the adsorption of pure ethane at 264.75 K, at high pressure, where the adsorbate density reflects the capacity of the adsorbent. (As we will see below, this isotherm—for the more strongly adsorbed component at the lowest experimental temperature—is the most structured and therefore the most demanding test of the model.) This adsorption isotherm was also used in an optimization process for the pore diameter and the Lennard-Jones parameter ϵ_O of the pore wall to get the best agreement between the experimental and the simulated adsorption isotherm. A pore diameter of 41 Å and ϵ_O/k_B = 185 K (where k_B is Boltzmann's constant) gave the best representation. (In contrast to the case of ref 31, it was not found necessary to use a distribution of values for ϵ_O.) The pore diameter corresponds to the value found with the BJH method (note, however, that the pore diameter used for the simulation is defined slightly differently from the experimental pore radius; see Figure 5). The corresponding porosity was 0.92 cm³/g, which is in line with the values given in refs 7 (0.5–1.0 cm³/g) and 57 (0.7–0.94 cm³/g).

5. Results and Discussion

5.1. Experimental Results. Pure-component equilibrium isotherms for methane and ethane on MCM-41 were measured over the temperature range from 265 to 373 K and at pressures up to 3.2 MPa. The experimental isotherms for these pure components are shown in Figure 6. (Also shown are the GCMC simulation results, which will be discussed later.) The adsorption experiment was repeated for each component (for a total of two adsorption runs for methane and three adsorption runs plus one desorption run for ethane) with a high degree of reproducibility (as shown in Figure 6). The rapid rise in the middle of the ethane isotherms at the two lowest temperatures reflects the near-critical state of ethane. The bulk critical temperature for ethane is 305.3 K. This is above the temperature of all but one of the ethane isotherms, but the critical temperature decreases with pore size.[58] The pores in the MCM-41 are evidently sufficiently small that pore filling occurs rapidly but continuously (the analogy in bulk vapor–liquid equilibrium being the high compressibility near the critical point). Methane (which has a critical temperature of 190.6 K) is supercritical by a substantial margin (even in the bulk) at all experimental temperatures and so does not exhibit this rapid rise, showing instead the IUPAC type I behavior characteristic of supercritical adsorption in microporous solids.

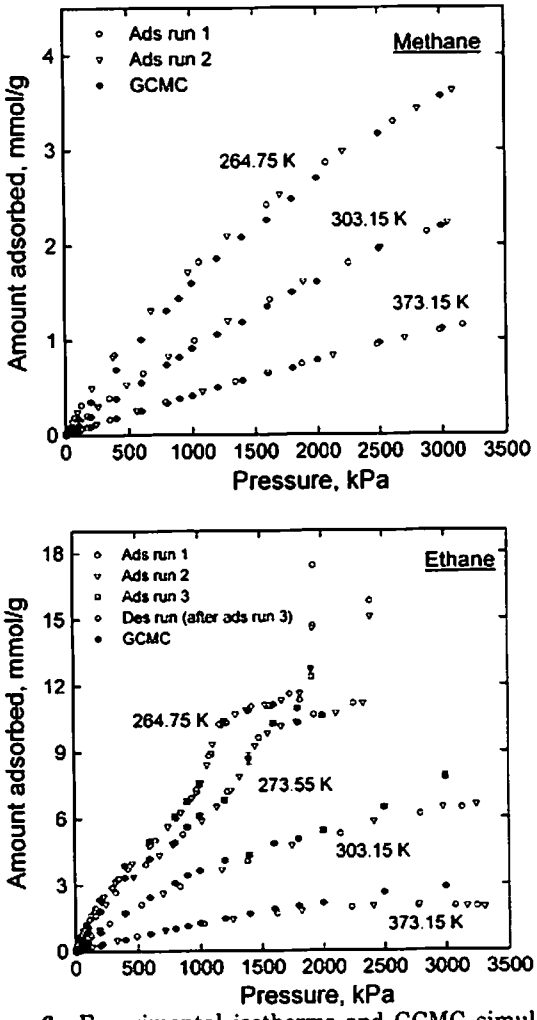

Figure 6. Experimental isotherms and GCMC simulation results for pure methane and ethane adsorption.

(56) Fischer, J.; Heinbuch, U.; Wendland, M. *Molec. Phys.* **1987**, *61*, 953.
(57) Goworek, J.; Stefaniak, W.; Borówka, A. *Stud. Surf. Sci. Catal.* **2000**, *128*, 207.
(58) Evans, R.; Marini Bettolo Marconi, U.; Tarazona, P. *J. Chem. Soc. Faraday Trans. 2* **1986**, *82*, 1763.

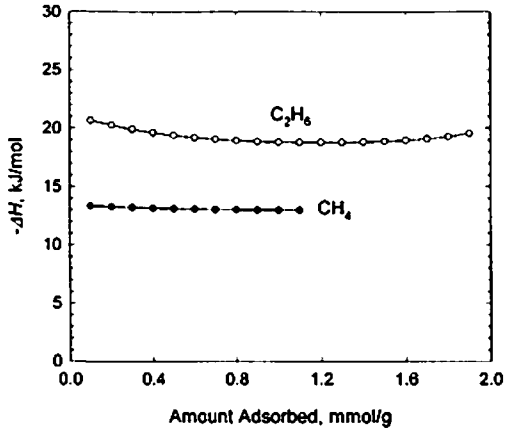

Figure 7. Isosteric heat data for pure methane and ethane adsorption.

The isosteric heat of adsorption at constant adsorbate loading, $-\Delta H_i$, was evaluated from pure-component equilibrium isotherm data by means of the Clausius–Clapeyron equation:[59]

$$-\Delta H_i = R\left(\frac{\partial \ln P}{\partial(1/T)}\right)_{n_i} \qquad (9)$$

where n_i is the number of moles of component i adsorbed. The resulting values of the isosteric heat are shown in Figure 7. The isosteric heat of methane adsorption is nearly constant (13.2 kJ/mol) within the loading range 0.1–1.1 mmol/g, suggesting that methane encounters a homogeneous adsorption potential. In contrast to the case for methane, the isosteric heat for ethane adsorption shows a slight dependence on the adsorbate loading within our experimental range (0.1–1.9 mmol/g). Initially, the isosteric heat decreases gently to an ethane loading of 1.2 mmol/g, indicating that there is some heterogeneity in the adsorption of ethane on the surface of MCM-41. Thereafter, the isosteric heat increases gradually with loading, presumably due to the increased importance of fluid–fluid interactions as the loading increases. However, the absolute variation in the isosteric heat for ethane is very small—only 2.5 kJ/mol within the experimental range—so even for this adsorptive the degree of heterogeneity is very low. The isosteric heat of ethane adsorption at zero loading is, by extrapolation, about 21.3 kJ/mol.

5.2. Prediction of Pure-Component Adsorption Using GCMC Simulation. Figure 6 shows the experimental isotherm data for pure methane and ethane, and the corresponding GCMC predictions. (As IAST is a solution thermodynamic model, based on a hypothetical mixing process, it provides no information about pure gas adsorption.) As indicated in Section 4, three parameters of the model MCM-41 (the porosity, the pore diameter, and ϵ_O) were fitted to the ethane isotherm at 264.75 K. No other adjustable parameters were used in the simulation, so the other simulated isotherms for ethane, and all the simulated isotherms for methane, are pure predictions. For ethane, the predictions are excellent for 273.55 K and become progressively poorer as the temperature rises. The error is largest for the highest temperature isotherm (373.15 K) at high pressure. Nevertheless, even under these conditions, the absolute error (which is what is relevant in predicting adsorption in technological applications) is quite small. The GCMC predictions of methane adsorption are highly accurate at the highest temperature and become progressively less accurate as the temperature decreases. Interestingly, the predictions are poorest at both low temperature and low pressure, perhaps reflecting the greater sensitivity to surface disorder—not represented in our model—which would be expected under these conditions. Overall, in terms of relative error, the methane adsorption is less accurately predicted by GCMC simulation. (The absolute error remains small, however, as methane adsorbs much more weakly than ethane.) This is not unexpected; the adjustable parameters (of what is, after all, a simplified model of the real adsorptives and adsorbent) were fitted to data for ethane, so with methane, one is making a greater extrapolation from the experimental data used to define the model.

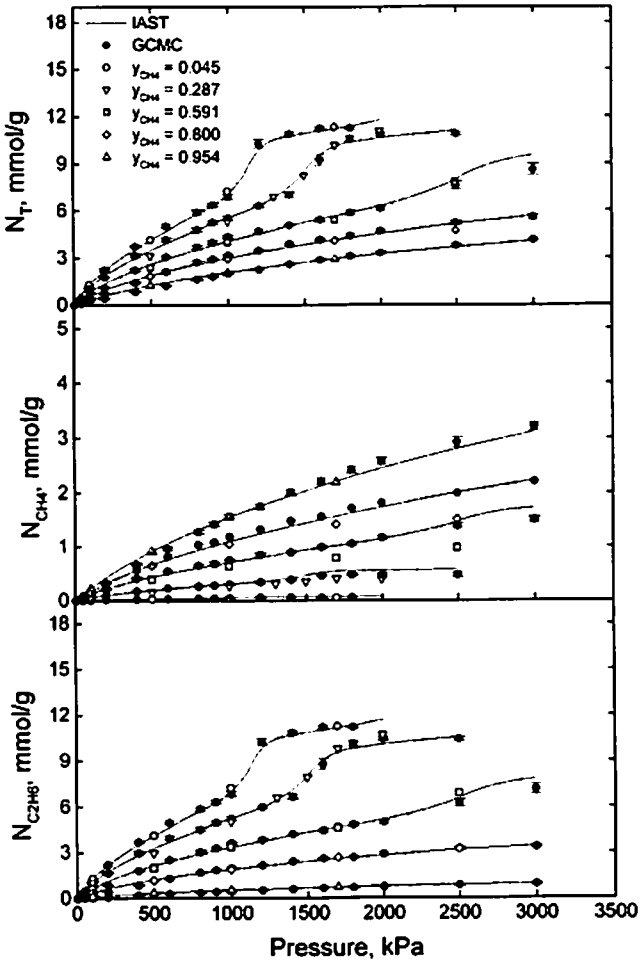

Figure 8. Adsorption equilibria for the binary mixtures at 264.75 K (constant gas composition path).

5.3. Prediction of Binary Adsorption Using IAST and GCMC Simulation. Figures 8 and 9 show experimental and predicted binary isotherms at 264.75 K, at constant gas composition and constant pressure, respectively. Both IAST and GCMC simulation accurately predict adsorption across the range of conditions. (The performance of IAST is significantly better than that in earlier results presented by the authors[60] in which the bulk phase was assumed to be an ideal gas, with pressure used instead of the fugacity in eqs 1 and 2; this illustrates the importance of taking into account gas-phase nonideality at high pressure.) It is particularly notable that both

(59) Hill, T. L. *J. Chem. Phys.* **1949**, *17*, 520.

(60) Yun, J. H.; Düren, T.; Seaton, N. A. In *Proceedings of the Seventh International Conference on the Fundamentals of Adsorption*; International Adsorption Society: in press.

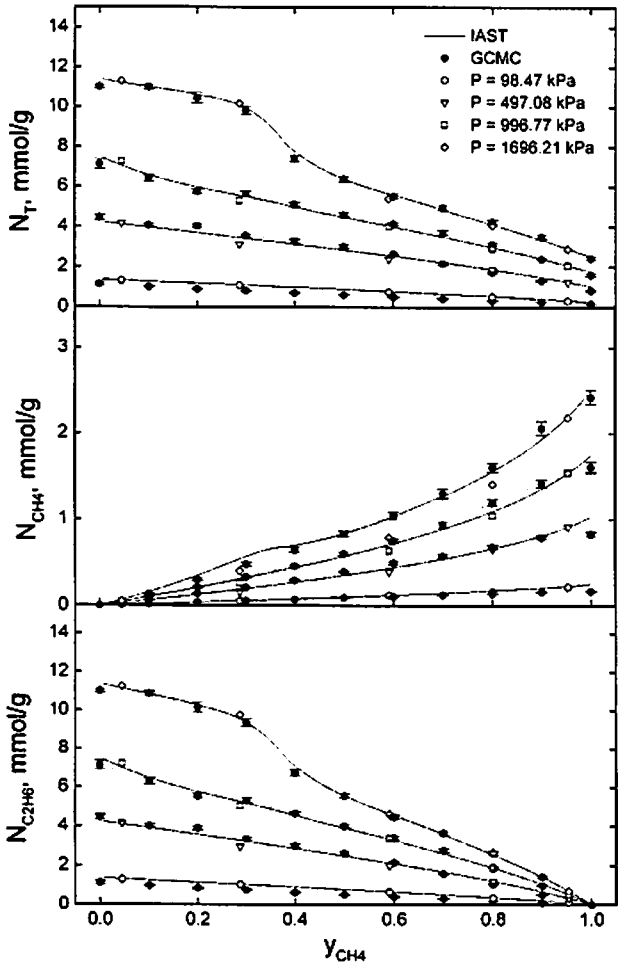

Figure 9. Adsorption equilibria for the binary mixtures at 264.75 K (constant gas pressure path).

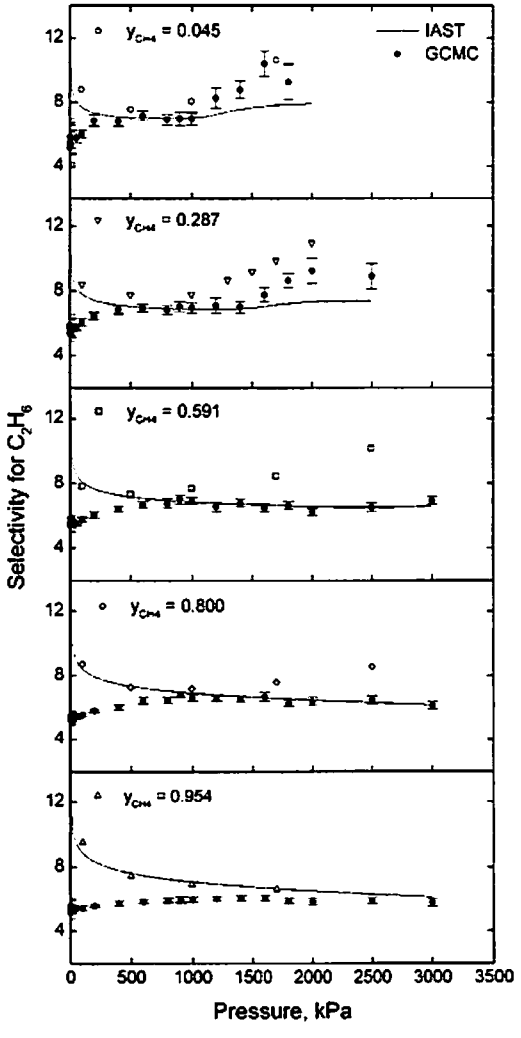

Figure 10. Adsorption selectivity for ethane relative to methane at 264.75 K (constant gas composition path).

methods accurately reproduce the rapid pore filling that is observed with ethane-rich mixtures. (The existence of this phenomenon in binary adsorption is, of course, not unexpected, as it was observed with pure ethane.)

Figure 10 shows the selectivity, S, defined by

$$S = \frac{x_{C_2H_6}/x_{CH_4}}{y_{C_2H_6}/y_{CH_4}} \qquad (10)$$

as a function of pressure, with bulk gas composition as a parameter, at 264.75 K. Figure 11 is the analogous plot with pressure as a parameter. As it contains the ratio of the adsorbed-phase mole fractions, the selectivity is a very sensitive measure of the accuracy of the prediction of the adsorbed-phase composition. These figures show that IAST accurately predicts the selectivity at low pressure, while GCMC simulation is significantly in error under these conditions. At higher pressure, the predictions of both GCMC simulation and IAST are relatively poor, except for ethane-rich mixtures at high pressure where GCMC simulation captures the experimental rise in selectivity. (The fact that GCMC simulation performs better for ethane-rich mixtures than for methane-rich mixtures reflects the relative performance of the method for the two pure components.) The performances of the two methods at low pressure are of particular interest. Because IAST uses the experimental pure-component isotherms as inputs, the Henry's-law limit (in which the selectivity is simply the ratio of the Henry's constants) is automatically reproduced by this method. It follows that the predicted selectivity at low pressure tends to be accurate in any IAST calculation. On the other hand, adsorption at low pressure is an area of vulnerability for GCMC simulation or any other predictive method based on a model of the pore structure. Our model has a regular array of oxygen atoms on the surface and misses the heterogeneity found in real MCM-41 because of the irregular arrangement of atoms and any defects present on the surface. These surface features are important at very low pressure, where adsorption is mostly directly on the surface, but of little significance at high pressure, where adsorption occurs in the bulk of the pore as well as on the surface. Thus, the GCMC predictions are less accurate at low pressure than at high pressure. Finally, it is worth pointing out that this weakness, while of interest from a scientific point of view, is of little relevance from a technological perspective, as the amounts adsorbed are very low at low pressure.

6. Conclusions

We have reported a comprehensive set of experimental data for the adsorption of methane, ethane, and mixtures of these components on MCM-41. We have demonstrated that IAST gives, overall, very accurate predictions of multicomponent adsorption equilibrium for this model system. This is, in principle, unsurprising; MCM-41 is a highly homogeneous adsorbent, consisting of an array of identical pores of constant cross section, and the methane/

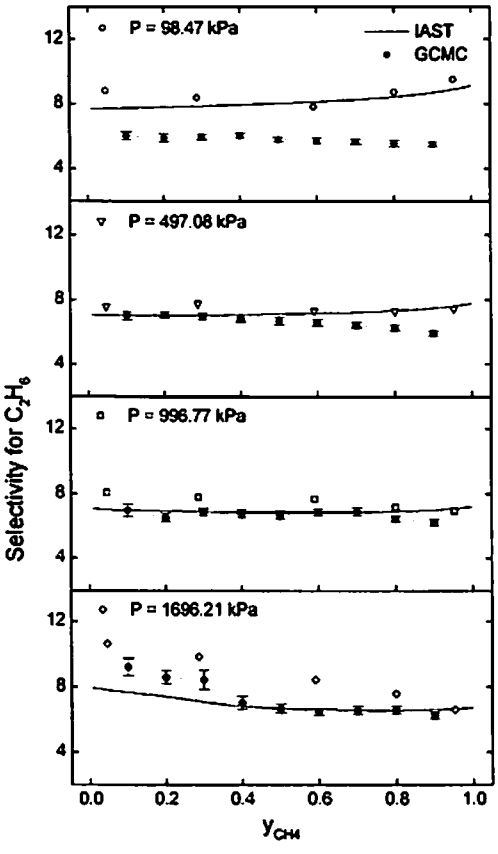

Figure 11. Adsorption selectivity for ethane relative to methane at 264.75 K (constant gas pressure path).

ethane mixture is highly ideal in the bulk. Nevertheless, the very high accuracy of IAST, and in particular the fact that it can quantitatively reproduce the rapid pore filling seen with ethane-rich mixtures, is noteworthy. This is a definitive demonstration of the validity of IAST at the level of individual pores.

The GCMC simulation method gives accurate predictions of both pure-component and binary adsorption in MCM-41, supporting the use of our simple model for MCM-41, which ignores surface heterogeneity. (Accurate prediction of the adsorbed-phase composition at low pressure, which is not achieved with this pore model, would require a model which correctly represented the type and degree of heterogeneity found experimentally.) The ability of GCMC simulation to accurately predict adsorption on MCM-41 supports the use of this method as a tool for the design of adsorbents. This is consistent with the good performance observed in earlier applications of GCMC simulation to the adsorption of nonpolar, or weakly polar, components and their mixtures on activated carbon, where the heterogeneity of the adsorbent is characterized by a pore size distribution and (if connectivity effects are important) the coordination number of the pore network.[41,61] As in the case of IAST, this study of adsorption in a model system serves to explain the observed success of the predictive method when applied to adsorption in heterogeneous adsorbents. Finally, we recall that all the GCMC predictions were based on a model with only three adjustable parameters (the porosity, the pore diameter, and ϵ_O) and that only one pure-component isotherm was needed to fix these parameters and to go on to predict pure and binary adsorption at different temperatures and with different fluids. GCMC simulation thus delivers accurate predictions over a wide range of conditions, with experimental inputs that are extremely modest compared with those for IAST and other thermodynamic methods.

Acknowledgment. The authors are grateful to G. Seo (Chonnam National University, Korea) for providing MCM-41 samples; to J. B. Parra Soto (Instituto Nacional del Carbon, Spain) for XRD and BET measurements; to P. M. Barata-Rodrigues for her contribution to the design and construction of the adsorption apparatus; and to E. Buss for his advice on the flow-through method. The financial support of the U. K. Engineering and Physical Sciences Research Council is gratefully acknowledged.

LA0155855

(61) Davies, G. M.; Seaton, N. A. *AIChE J.* **2000**, *46*, 1753.